CHAPTER 1

# Determination of Photoadsorption Capacity of Polychrystalline $TiO_2$ Catalyst in Irradiated Slurry

**Vincenzo Augugliaro**[1,*], **Sedat Yurdakal**[1,2], **Vittorio Loddo**[1], **Giovanni Palmisano**[1], and **Leonardo Palmisano**[1]

Contents



[1] "Schiavello-Grillone" Photocatalysis Group, Dipartimento di Ingegneria Chimica dei Processi e dei Materiali, Università di Palermo, Viale delle Scienze, 90128 Palermo, Italy

[2] Kimya Bölümü, Fen Fakültesi, Anadolu Üniversitesi, Yunus Emre Kampüsü, 26470 Eskişehir, Turkey

[*] Corresponding author.
*E-mail address*: augugliaro@dicpm.unipa.it

Advances in Chemical Engineering, Volume 36
ISSN 0065-2377, DOI: 10.1016/S0065-2377(09)00401-3

## 1. INTRODUCTION

In the field of heterogeneous catalysis the need of kinetic investigation is strictly connected to the main task of a chemical engineer, that is, designing properly a chemical reactor. A successful reactor design should thus start from reliable kinetic models that describe the rate of catalytic reactions and, therefore, from the reaction mechanisms, which means understanding reactions at a molecular level. In catalysis, due to the complex nature of this phenomenon, adsorption and desorption of reactants as well as several steps for surface reactions must be taken into account. For heterogeneous photocatalysis, which may be considered a special case of heterogeneous catalysis, the previous considerations hold true with the added difficulty that the light absorbed by the photocatalyst affects both adsorption (photoadsorption) and surface reactions.

The use of irradiation to initiate chemical reactions is the principle on which heterogeneous photocatalysis is based. When a wide band gap semiconductor like titanium dioxide (Carp et al., 2004) is irradiated with suitable light, excited electron–hole pairs result that can be applied in chemical processes to modify specific compounds. If recombination or lattice reaction does not involve all the photogenerated pairs, the conduction band electrons participate in reduction reactions on the catalyst surface while positive holes are involved in oxidation reactions. Suitable substrates must be adsorbed on the catalyst surface for the occurrence of a photoreaction process which always starts with the substrate(s) adsorption and eventually ends with the product(s) desorption. On these grounds heterogeneous photocatalysis is defined as follows (Braslavsky, 2007): "*Change in the rate of a chemical reaction or its initiation under the action of ultraviolet, visible, or infrared radiation in the presence of a substance, the photocatalyst, that absorbs light and is involved in the chemical transformation of the reaction partners.*" Symbolically overall photocatalytic reaction is expressed by the equation:

$$R + \mathrm{Cat} + h\nu \rightarrow P + \mathrm{Cat} \tag{1}$$

where $R$ and $P$ are reactants and reaction products, respectively, present in the gas or liquid phase, Cat is the solid photoadsorbent (photocatalyst), and $h\nu$ is the symbol of photons able to be absorbed by the photocatalyst.

The knowledge of heterogeneous photocatalytic systems has grown very much since the pioneering work on water photolysis carried out with a semiconductor electrode (Fujishima and Honda, 1972). The basic principles of heterogeneous photocatalysis are now well established (Fujishima et al., 1999; Kaneko and Okura, 2002; Schiavello, 1997) and also the applicative aspects of this technology are being investigated in the fields not only of environment remediation (Augugliaro et al., 2006; Fujishima et al., 2000; Mills and Le Hunte, 1997) but also of green chemistry (Gonzalez et al., 1999; Mohamed et al., 2002; Yurdakal et al., 2008a). There are, however, many

important aspects waiting to be investigated. One of these is the correct approach for the determination of the photoadsorption capacity under photoprocess occurrence, that is, of the amount of substrate adsorbed on the surface of a photocatalyst which is being irradiated.

Photon absorption by photocatalyst is regarded as the first stage of photoexcitation of heterogeneous system; the photoexcitation pathways of wide band gap solids may involve photogeneration of excitons and/or free charge carriers, depending on photocatalyst features such as fundamental absorption band, extrinsic/intrinsic defect absorption bands, or UV-induced color center bands. Independently of photoexcitation type, photon absorption has two main effects: (i) it changes the characteristics of photocatalyst surface and (ii) it generates active photoadsorption centers. A typical case of the first effect is that band gap irradiation induces superhydrophilicity (photoinduced superhydrophilicity, PSH) on the $TiO_2$ surface, which shows hydrophobic features under dark conditions (Fujishima and Zhang, 2006; Fujishima et al., 2000; Wang et al., 1997). This PSH is accompanied by photocatalytic activity, as both phenomena have a common ground, so that the surface-adsorbed compounds may be either photooxidized or washed away by water.

The second important effect is that irradiation absorption generates active states of the photoadsorption centers with trapped electrons and holes. By definition (Serpone and Emeline, 2002) "*the photoadsorption center is a surface site which reaches an active state after photoexcitation and then it is able to form photoadsorbed species by chemical interaction with substrate (molecules, or atoms, or ions) at solid/fluid interface.*" In turn, the active state of a surface photoadsorption center is "*an electronically excited surface center, i.e. surface defect with trapped photogenerated charge carrier that interacts with atoms, molecules or ions at the solid/gas or solid/liquid interfaces with formation of chemisorbed species.*"

Adsorption initiated by light absorbed by the solid surface (photoadsorption) can be expressed by the following simple mechanism (Ryabchuk, 2004):

$$S + h\nu \rightarrow S^* \tag{2}$$

$$S^* \rightarrow S \tag{3}$$

$$S^* + M \rightarrow M_{p\text{-}ads} \tag{4}$$

where S is the photoadsorption center, $S^*$ the active state of photoadsorption center, M the substrate in the fluid phase, and $M_{p\text{-}ads}$ the photoadsorbed substrate. Equation (2) describes the photoexcitation of adsorbent with formation of active $S^*$ centers and Equation (4) the adsorption of molecule M or "chemical decay" of the active states $S^*$, while Equation (3) depicts the "physical decay" of $S^*$ state.

For a liquid–solid catalytic reaction the common technique for determining the adsorbed amount of a species dissolved in the solution is that of performing experiments in a batch not-reacting system and of measuring: (i) the volume of liquid solution; (ii) the concentration of the adsorbing species in the starting solution; and (iii), after that a known mass of catalyst is added to the liquid and steady-state conditions are reached, the concentration decrease determined in the starting solution due to the added catalyst. This procedure is based on the adequate assumptions that the catalyst's superficial features are not affected by the composition of the surrounding fluid phase and that the measured decrease of the species amount in the solution is equal to the amount of species adsorbed on the catalyst. The same procedure cannot be applied for the photoadsorption determination; in fact, photoadsorption occurs under the simultaneous presence of irradiation and of reducing and oxidizing species needed for charge carriers to be trapped on the semiconductor surface. Under these conditions the photoreaction also starts so that the measured decrease of species in the batch-irradiated slurry is determined both by photoadsorption and by reaction, these contributions being indistinguishable from the solution side.

This complexity determines that investigations on heterogeneous photocatalytic processes sometimes report information only on dark adsorption and use this information for discussing the results obtained under irradiation. This extrapolation is not adequate as the characteristics of photocatalyst surface change under irradiation and, moreover, active photoadsorption centers are generated. Nowadays very effective methods allow a sound characterization of bulk properties of catalysts, and powerful spectroscopies give valuable information on surface properties. Unfortunately information on the photoadsorption extent under real reaction conditions, that is, at the same operative conditions at which the photoreactivity tests are performed, are not available. For the cases in which photoreaction events only occur on the catalyst surface, a critical step to affect the effectiveness of the transformation of a given compound is to understand the adsorption process of that compound on the catalyst surface. The study of the adsorbability of the substrate allows one to predict the mechanism and kinetics that promote its photoreaction and also to correctly compare the performance of different photocatalytic systems.

This chapter presents a quantitative method to determine the photoadsorption capacity of a polycrystalline semiconductor oxide irradiated in liquid–solid system. The determination is performed under reaction conditions so that it is really indicative of the photoadsorption capacity. The method uses the experimental results obtained in typical batch photoreactivity runs; on this ground it has been applied to the following photocatalytic processes carried out in aqueous suspensions: (i) oxidation of phenol in the presence of a commercial $TiO_2$ catalyst (Degussa P25) and (ii) oxidation of benzyl alcohol in the presence of a home-prepared $TiO_2$

catalyst. The influence on photoactivity of substrate concentration, catalyst amount, and irradiation power is investigated. The kinetic modeling of the photooxidation processes is carried out by taking into account the photoadsorption phenomenon by means of three types of isotherm equations, that is, Langmuir, Freundlich, and Redlich–Peterson. Nonlinear regression analysis applied to all the photoreactivity results allows establishing the most appropriate correlation for the photoadsorption isotherm and also to determine the values of the model parameters. The best fitting model is evaluated by choosing the Marquardt's percent standard deviation (MPSD) as error estimation tool.

## 2. EXPERIMENTAL

Photoreactivity runs of phenol degradation were carried out in aqueous suspensions of a commercial $TiO_2$ (Degussa P25) while for benzyl alcohol degradation a home-prepared nanostructured $TiO_2$ specimen was used. The preparation method of home-prepared catalyst is summarized here; the details are elsewhere reported (Addamo et al., 2004). The precursor solution was obtained by slowly adding 5 mL of $TiCl_4$ drop by drop into a 200-mL beaker containing 50 mL of water; during the addition, which lasted 5 min, the solution was magnetically stirred by a cylindrical bar (length, 3 cm; diameter, 0.5 cm) at 600 rpm. After that the beaker was closed and mixing was prolonged for 12 h at room temperature, eventually obtaining a clear solution. This solution was transferred to a round-bottom flask having on its top a Graham condenser (Palmisano et al., 2007a). The flask was put in boiling water, thus determining the boiling of the solution; the duration of the boiling was of 0.5 h, obtaining a white suspension at the end of the treatment. The suspension was then dried at 323 K by means of a rotovapor machine (model Buchi Rotovapor M) working at 150 rpm, in order to obtain the final powdered, poorly crystalline anatase-phase catalyst.

The flow-sheet of the experimental setup is shown in Figure 1. The details are reported elsewhere (Palmisano et al., 2007b). A cylindrical batch photoreactor of Pyrex glass with immersed lamp was used for the photocatalytic runs of benzyl alcohol and phenol oxidation. On the top of the reactor three ports allowed the inflow and outflow of gases, the pH and temperature measurements, and the withdrawal of samples for analysis.

The catalyst was used in aqueous suspension well mixed by means of a magnetic stirrer. The reacting mixture was illuminated by a mercury medium-pressure lamp (type B, Helios Italquartz, Milan, Italy) coaxial with the photoreactor. A Pyrex thimble surrounding the lamp allowed the circulation of distilled water in order to cool the lamp and cutoff infrared radiation; in these conditions the reactor temperature was of $295 \pm 2$ K. Lamps of 125, 500, or 1,000 W electric power were used; average irradiances

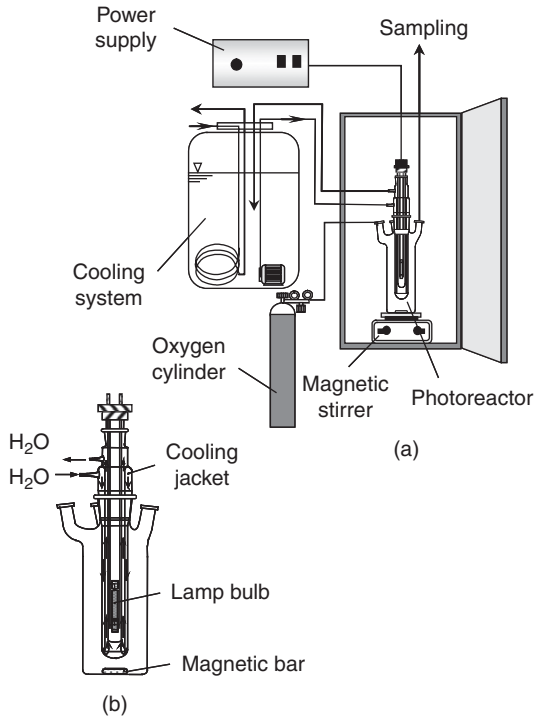


**Figure 1** (a) Set up of experimental apparatus and (b) Photoreactor (Palmisano et al., 2007b).

impinging onto and leaving the suspension were measured by using a radiometer (UVX, Digital) at $\lambda = 360$ nm; these measurements were carried out for each lamp and each catalyst concentration. By considering that the lamp thimble does not transmit radiation with wavelength less than 300 nm and that the lamps mainly emit at 310 and 360 nm, the previous measurements were allowed to have an estimate of the photon flow absorbed by the suspension. These values, even if they are approximate, are however useful in quantitatively ordering the different suspensions with respect to their ability in absorbing photons. The benzyl alcohol and phenol initial concentrations varied in the 0.5–5.0 and 0.25–4.0 mM ranges, respectively, and the catalyst amounts were in the 0.05–0.8 g $L^{-1}$ range.

The standardized procedure of the runs was the following one and it was strictly observed; the procedure stages are depicted in Figure 2. The photoreactor *without the immersed lamp* was filled with a fixed volume of substrate aqueous solution of known concentration and pure oxygen (or air for a few runs) was bubbled for 30 min under magnetic stirring (bubbling and stirring were never interrupted in the course of runs); then the desired amount of catalyst was added and samples (5 $cm^3$) of the suspension were taken at

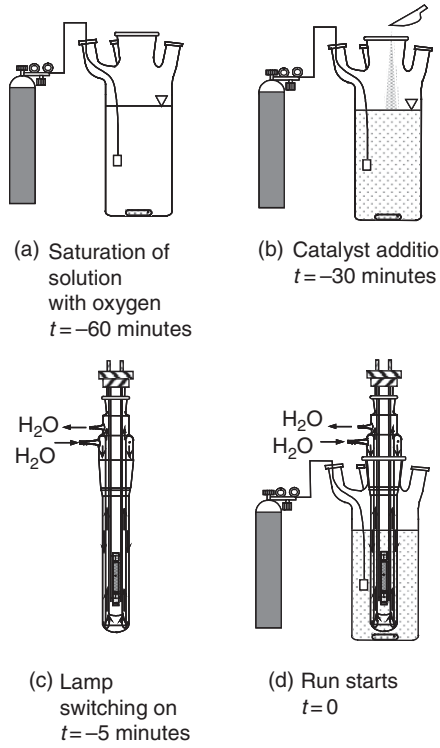


**Figure 2** Experimental run procedure from (a) to (d).

fixed intervals of time until the dark equilibrium conditions were reached (about 30 min after catalyst addition). At that time the lamp *outside the photoreactor* was switched on and time was allowed for reaching steady-state conditions of irradiation (about 5 min). Once the irradiation did not change, as checked by the radiometer, the lamp was fast immersed into the suspension and that time was taken as the zero time of the photoreactivity run; samples (5 $cm^3$) for analysis were withdrawn by means of a syringe every 15 min in the first 2 h of the run and then every 0.5 or 1 h. The samples were immediately filtered by inserting a cellulose acetate filter (Millipore, Billerica, MA USA, pore diameter of 0.45 μm) on the exit hole of the sampling syringe.

For benzyl alcohol degradation runs the quantitative determination and identification of the species present in the reacting suspension was performed by means of a high-performance liquid chromatograph (HPLC) (Beckman Coulter, Fullerton, CA USA, System Gold 126 Solvent Module and 168 Diode Array Detector), equipped with a Luna 5 μ Phenyl–Hexyl column (250 mm long × 2 mm i.d.) using standards (Sigma-Aldrich, St. Louis, MO USA). The eluent consisted of 17.5% acetonitrile, 17.5% methanol, 65% 40 mM $KH_2PO_4$ aqueous solution. For phenol degradation

runs the quantitative determination and identification was performed by using the same HPLC and the eluent consisted of 35% methanol and 65% 40 mM $KH_2PO_4$ aqueous solution.

For TOC determinations 2 $cm^3$ of the irradiated slurry was withdrawn from the photoreactor every 30 min and, after filtration over the Millipore filter, analyzed by a TOC Shimadzu analyzer.

All the used chemicals (Sigma-Aldrich) had a purity $> 99.0\%$.

## 3. $TiO_2$ SURFACE MODIFICATIONS UNDER IRRADIATION

For gas–solid and liquid–solid systems, the interaction of a species with the solid surface depends on the chemical nature of the species and on the chemical and physical nature of the solid. For nonilluminated surface of semiconductor oxides, a thermodynamic equilibrium between a species and the solid is established only when the electrochemical potential of the electrons in the entire system is uniform. When the adsorption–desorption equilibrium is established, an aliquot of the species is located in an adsorbed layer, held at the surface by either weak or strong bonding forces.

When a photocatalyst goes from dark conditions into irradiated ones, the radiation absorption determines that its surface undergoes a series of changes needed for eventually allowing the occurrence of photoprocesses (Bickley, 1985a, b). Essentially the interaction of a photon with a solid semiconductor gives rise to an increase of the vibrational state of the lattice or the number of quasi-free charge carriers, that is, it generates an excited state of the solid. The illumination with band gap (or greater) energy creates a perturbation to this adsorption–desorption equilibrium established in the dark; under irradiation the previous equilibrium is displaced determining a net photoadsorption or photodesorption of species. A new equilibrium is achieved when the species and the solid acquire the same electrochemical potential (Bickley, 1988a, b).

Direct observation of photosorption phenomena at the $TiO_2$ surface has been reported in several earlier studies, focussing on the role played by surface OH groups in the photoadsorption of oxygen and therefore in regulating the $TiO_2$ photoactivity. For example, UV illumination stimulates desorption of oxygen and water molecules adsorbed at the $TiO_2$ surface (Meriaudeau and Vedrine, 1976; Murphy et al., 1976; Sakai et al., 1998; Wang et al., 1999; Wu et al., 2000) while studies by IR and XPS reveal that the amount of OH groups on the $TiO_2$ surface increases by UV illumination (Asakuma et al., 2003; Hoffmann et al., 1995; Ignatchenko et al., 2006; Linsebigler et al., 1995; Mori et al., 2007). These changes are generally fast and reversible, that is, once irradiation is stopped the surface recovers its previous features, at equal initial conditions. A well-recognized indication of the fact that irradiation modifies the surface of wide band gap solids is

the post-sorption or memory effect, that is, the adsorption in the dark caused by the pre-irradiation of solid surface (Solonitzyn and Terenin, 1959; Solonitzyn et al., 1982).

A more recent and clear evidence of this behavior is the phenomenon of induced superhydrophilicity, that is, the generation of a highly hydrophilic $TiO_2$ surface by UV illumination (Lee et al., 2003; Miyauchi et al., 2002; Nakajima et al., 2001; Sakai et al., 1998; Takeuchi et al., 2005; Wang et al., 1997; Watanabe et al., 1999). Superhydrophilic property of the $TiO_2$ surface allows water to spread completely across the surface rather than remaining as droplets. In the case of a film which consists of only $TiO_2$, the contact angle of water almost becomes zero during UV irradiation. However, it is found that the contact angle goes up and is restored comparatively quickly in a dark place. One of the most interesting aspects of $TiO_2$ is that photocatalysis and induced hydrophilicity can take place simultaneously on the same surface even though the mechanisms are different. In the case of photocatalysis, UV light excites the catalyst and pairs of electrons and holes are generated; the photogenerated electrons then react with molecular oxygen to produce superoxide radical anions and the photogenerated holes react with water to produce hydroxyl radicals. These two types of rather reactive radicals then work together to carry out redox reactions with species adsorbed on the $TiO_2$ surface. On the other hand, surface hydroxyl groups can trap more photogenerated holes and improve the separation of electrons and holes which results in the enhancement of photocatalysis.

In the case of superhydrophilicity electrons and holes are still produced, but they react in a different way. The electrons tend to reduce the Ti(IV) cations to the Ti(III) state, and the holes oxidize the oxygen anions. In the process, oxygen atoms are ejected, creating oxygen vacancies. Water molecules can then occupy these oxygen vacancies, producing adsorbed OH groups, which tend to make the surface hydrophilic. Depending upon the composition and the processing, the surface can have more photocatalytic character and less superhydrophilic character, or vice versa. In spite of the different mechanism of photocatalytic and hydrophilic effect, they behave synergetically. Because more OH groups can be adsorbed on the surface due to hydrophilicity, the photocatalytic activity is enhanced; so hydrophilicity can improve photocatalysis. On the other hand, the surface can adsorb contaminated compounds which tend to turn the hydrophilic surface to hydrophobic surface. Photocatalysis can decompose the organic compounds on the surface resulting in the restoration of hydrophilicity. From this point, photocatalysis can improve hydrophilicity and maintain this characteristic for a long time. The proposed mechanism means that the surface structure changes during the reaction. In other words, the rate of photo-induced hydrophilicity may depend on the history of the sample.

Specifically for liquid–solid systems, adsorption phenomena involving ions occur with a transfer of electric charge, causing a significant variation of the electronic band structure of the surface. The charge transfer is responsible for the formation of the so-called space-charge layer where the potential difference between surface and bulk creates an electric field that can play a beneficial role in the further adsorption steps. Most photons are absorbed in the superficial layer of the solid where the space-charge exists and the photoelectrons straightforwardly interact with the electric field present here. The consequence is a more efficient separation of the electrons and holes within the space-charge layer, that is, the increase of their mean lifetime.

Photoadsorbed species can act (i) as surface-hole trapping and photoelectrons can be trapped in the bulk of the solid or (ii) as surface-electron trapping and holes can react with OH surface groups and/or $H_2O$. Both the alternatives depend on the chemical nature of the molecule to be adsorbed and on the type of the solid adsorbent. It is worth noting that in the gas–solid regime only gaseous species or lattice ions can be involved, whereas in the liquid phase also the interaction with the solvent (often $H_2O$) should also be considered.

All the above considerations allow to conclude that the electronic surface modifications created under irradiation eventually induce photoadsorption both in gas–solid and in liquid–solid regimes, being the photoadsorption phenomenon strictly related with the photoactivity of the solid photocatalysts. When light is switched off, a reversal of the process could be observed, although rarely the reversibility is complete and the achievement of a new equilibrium depends mainly on kinetics rather than thermodynamic factors.

## 4. PHOTOADSORPTION DETERMINATION

For heterogeneous photocatalytic processes, it is generally agreed that the expression for the degradation rate of organic substrates on $TiO_2$ surfaces in the presence of oxygen follows (with minor variations) the Langmuir–-Hinshelwood (LH) model, which is widely used in liquid- and gas-phase systems (de Lasa et al., 2005; Gora et al., 2006; Ibrahim and de Lasa, 2004; Murzin and Salmi, 2005; Palmisano et al., 2007c; Turchi and Ollis, 1989; Vorontsov et al., 1999). This model successfully explains the kinetics of reactions that occur between two adsorbed species, a free radical and an adsorbed substrate, or a surface-bound radical and a free substrate. In the LH model, adsorption equilibrium is assumed to be established at all times so that the rate of reaction is taken to be much less than the rate of adsorption or desorption. Reaction is assumed to occur between adsorbed species whose coverage on the catalyst surface is always in equilibrium with the

species concentration in the fluid phase so that the rate-determining step of the photocatalytic process is the surface reaction. The concentrations of adsorbed species are therefore determined by adsorption equilibrium as given by the suitable isotherm. It is useful to report that the simple rate form of the LH approach may have origins which take into account different photoreaction mechanisms (Demeestere et al., 2004; Krýsa et al., 2006; Minero and Vione, 2006).

In batch photocatalytic reactors working in liquid–solid regime, the depletion of a species is the combined result of photoadsorption and photoconversion processes. To describe this depletion, a mole balance applied to the species at whatever time (de Lasa et al., 2005) can be represented as

$$n_T = n_L + n_S \tag{5}$$

where $n_T$ is the total number of moles present in the photoreactor, $n_L$ the number of moles in the fluid phase, and $n_S$ the number of moles photoadsorbed on the solid. When Equation (5) is divided by the volume of the liquid phase, $V$, one obtains:

$$C_T = C_L + \frac{n_S}{V} \tag{6}$$

where $C_T$ is the total concentration of the species and $C_L$ the concentration in the liquid phase.

By considering that both substrate and oxygen must be present in the system for the occurrence of photoreaction, it is assumed that the total disappearance rate of substrate per unit surface area, $r_T$, follows a second-order kinetics of first order with respect to the substrate coverage and of first order with respect to the oxygen coverage:

$$r_T \equiv -\frac{1}{S}\frac{dn_T}{dt} = k''\theta_{Sub}\theta_{Ox} \tag{7}$$

in which $S$ is the catalyst surface area, $t$ the time, $k''$ the second-order rate constant, and $\theta_{Sub}$ and $\theta_{Ox}$ are the substrate and oxygen fractional coverages of the surface, respectively. $\theta_{Sub}$ and $\theta_{Ox}$ are defined in the following way:

$$\theta_{Sub} \equiv \frac{n_S}{WN_S^*} \tag{8}$$

$$\theta_{Ox} \equiv \frac{n_{S,Ox}}{WN_{S,Ox}^*} \tag{9}$$

where $n_{S,Ox}$ is the number of oxygen moles photoadsorbed on the solid, $N_S^*$ and $N_{S,Ox}^*$ are the maximum capacity of photoadsorbed moles of substrate

and oxygen, respectively, on the unit mass of irradiated solid, and $W$ the mass of catalyst.

By considering that in the course of the runs the oxygen bubbling in the dispersion is not stopped, its concentration in the liquid phase does not change during the occurrence of substrate degradation and, moreover, it is always in excess. Then the $\theta_{Ox}$ term of Equation (7) does not depend on time, that is, it is a constant. By putting $k = k'' \cdot \theta_{Ox}$, Equation (7) turns a pseudo-first-order rate equation:

$$r_T \equiv -\frac{1}{S}\frac{dn_T}{dt} = k\theta_{Sub} \tag{10}$$

in which $k$ is the pseudo-first-order rate constant. Introducing in Equation (10) the liquid volume, $V$, and the surface area per unit mass of catalyst, $S_S$, one obtains

$$r_T \equiv -\frac{1}{S}\frac{dn_T}{dt} = -\frac{1}{S_S W}V\frac{dC_T}{dt} = k\theta_{Sub} \tag{11}$$

By considering that the kinetic information on the photoprocess consists on the knowledge of substrate concentration values in the liquid phase, $C_L$, as a function of irradiation time, the $C_T$ and $\theta_{Sub}$ variables of Equation (11) must to be transformed as a function of $C_L$. With concern to $\theta_{Sub}$, it is necessary to choose an adsorption isotherm, that is, a relationship between $\theta_{Sub}$ [and therefore $n_S$, see Equation (8)] and $C_L$, while for $C_T$ Equation (6) coupled with the chosen isotherm may be used. Therefore, Equation (11) may be formally written in the following way:

$$-\frac{1}{S_S W}V\frac{d}{dt}C_T(C_L) = k\theta_{Sub}(C_L) \tag{12}$$

It is important to remind that the kinetic modeling is carried out by assuming that the main assumptions of the LH model hold; it means that Equation (12) gives the evolution with irradiation time of the concentration in the liquid phase, $C_L$, of a species which is in photoadsorption equilibrium on the catalyst surface over which the species undergoes a slow transformation process. The main implication of the previous statement is that for a batch photocatalytic run the substrate concentration values measured in the liquid phase at a certain time represent the substrate concentration in equilibrium with an (unknown) substrate amount photoadsorbed on the catalyst surface. This feature belongs to all the measured values of substrate concentration except to the initial one. The substrate concentration measured at the start of a photoreactivity run is characteristic of a system without irradiation. As a consequence, when a kinetic model is fitted to the experimental data, the

regression analysis must be done with the concentration values measured in the course of the run excluding the value of initial substrate concentration because the condition of the initial concentration value (dark) is not that of the other ones (irradiated) (Yurdakal et al., 2008b).

## 4.1. Langmuir isotherm

The Langmuir isotherm theory (Satterfield, 1980) assumes a monolayer coverage of adsorbate over a homogenous adsorbent surface. A plateau characterizes the Langmuir isotherm; therefore, a saturation point is reached where no further adsorption can occur. Adsorption is assumed to take place at specific homogeneous sites within the adsorbent. Once a molecule occupies a site, no further adsorption can take place at that site. The Langmuir model assumes that the catalyst surface is completely uniform, that is, (i) the adsorption onto the surface of each molecule has equal activation energy and (ii) no transmigration of adsorbate in the plane of the surface occurs. Those assumptions are hypothesized here to be suitable to describe also photoadsorption. The Langmuir adsorption isotherm is described by the following relationship:

$$\theta_{\mathrm{Sub}} \equiv \frac{n_{\mathrm{S}}}{WN_{\mathrm{S}}^{*}} = \frac{K_{\mathrm{L}}^{*}C_{\mathrm{L}}}{1 + K_{\mathrm{L}}^{*}C_{\mathrm{L}}} \tag{13}$$

where $K_{\mathrm{L}}^{*}$ is the photoadsorption equilibrium constant, which is related to the free energy of photoadsorption, and $N_{\mathrm{S}}^{*}$ the monolayer adsorption capacity. $K_{\mathrm{L}}^{*}$ may be considered a measure of the intrinsic photoreactivity of the catalyst surface. By solving Equation (13) with respect to $n_{\mathrm{S}}$ and substituting in Equation (6), the result is

$$C_{\mathrm{T}} = C_{\mathrm{L}} + \frac{WN_{\mathrm{S}}^{*}}{V}\frac{K_{\mathrm{L}}^{*}C_{\mathrm{L}}}{1 + K_{\mathrm{L}}^{*}C_{\mathrm{L}}} \tag{14}$$

Substituting in Equation (11), the Langmuir relationship [Equation (13)] produces

$$-\frac{V}{WS_{\mathrm{S}}}\frac{\mathrm{d}C_{\mathrm{T}}}{\mathrm{d}t} = k\frac{K_{\mathrm{L}}^{*}C_{\mathrm{L}}}{1 + K_{\mathrm{L}}^{*}C_{\mathrm{L}}} \tag{15}$$

Taking the derivative of Equation (14) with respect to time, it yields

$$\frac{\mathrm{d}C_{\mathrm{T}}}{\mathrm{d}t} = \left[1 + \frac{W\,N_{\mathrm{S}}^{*}K_{\mathrm{L}}^{*}}{V}\frac{1}{(1 + K_{\mathrm{L}}^{*}C_{\mathrm{L}})^{2}}\right]\frac{\mathrm{d}C_{\mathrm{L}}}{\mathrm{d}t} \tag{16}$$

Substituting Equation (16) in the left-hand side term of Equation (15), one obtains

$$-\frac{V}{WS_S}\left[1+\frac{WN_S^*K_L^*}{V}\frac{1}{(1+K_L^*C_L)^2}\right]\frac{dC_L}{dt}=k\frac{K_L^*C_L}{1+K_L^*C_L} \tag{17}$$

and, rearranging and separating the variables, the following differential equation is obtained:

$$-\frac{V}{WS_S}\frac{1}{kK_L^*}\frac{dC_L}{C_L}-\frac{V}{WS_S}\frac{1}{k}dC_L-\frac{1}{S_S}\frac{N_S^*}{k}\frac{dC_L}{C_L(1+K_L^*C_L)}=dt \tag{18}$$

As outlined before, Equation (18) gives the evolution with irradiation time of the concentration in the liquid phase of a species which is in photoadsorption equilibrium on the catalyst surface over which the species undergoes a slow transformation process. On this ground, the integration of Equation (18) must be performed with the condition that at $t=0$ the substrate concentration in the liquid phase is that in equilibrium with the initial photoadsorbed amount, $C_{L,0}$; this initial concentration is unknown but it may be determined by the regression analysis carried out with the experimental data obtained after the start of irradiation. The integration yields

$$\frac{V}{WS_S}\frac{1}{kK_L^*}\ln\frac{C_{L,0}}{C_L}+\frac{V}{WS_S}\frac{1}{k}(C_{L,0}-C_L)+\frac{1}{S_S}\frac{N_S^*}{k}\ln\left(\frac{1+K_L^*C_L}{1+K_L^*C_{L,0}}\frac{C_{L,0}}{C_L}\right)=t \tag{19}$$

Equation (19) contains four unknown parameters, $K_L^*$, $N_S^*$, $k$, and $C_{L,0}$, whose determination may be carried out by a best fitting procedure.

## 4.2. Freundlich isotherm

The Langmuir theory of adsorption is an approximation of the real surfaces as surface reconstruction frequently occurs. An assumption generally used for the description of the physical chemistry of real adsorbed layers is that surface sites are different, the so-called biographical nonuniformity (Murzin and Salmi, 2005). By applying the Langmuir adsorption isotherm to a distribution of energies among the sites such that the heat of adsorption decreases logarithmically with coverage, the Freundlich isotherm is derived (Satterfield, 1980); it is described by the following relationship:

$$\theta_{Sub}\equiv\frac{n_S}{WN_S^*}=K_F^*C_L^{1/n} \tag{20}$$

where $K_F^*$ is the Freundlich isotherm constant indicative of the relative adsorption capacity of the adsorbent and $n$ a dimensionless parameter

indicative of the intensity of the adsorption. The $n$ parameter represents the mutual interaction of adsorbed species; a value of $n$ greater than unity is interpreted to mean that adsorbed molecules repulse one another. The Freundlich expression is an exponential equation and therefore it assumes that as the adsorbate concentration in the liquid phase increases, the concentration of adsorbate on the adsorbent surface also increases. Using the empirical form of Freundlich isotherm, an infinite amount of adsorption can occur, what is contrary to chemisorption. The statistical derivation of this isotherm, however, sets a value of the Freundlich maximum adsorption capacity, $N_S^*$. By solving Equation (20) with respect to $n_S$ and substituting in Equation (6), the result is

$$C_T = C_L + \frac{WN_S^*}{V} K_F^* C_L^{1/n} \tag{21}$$

Substituting in Equation (11) the Freundlich relationship [Equation (20)] produces

$$-\frac{V}{WS_S}\frac{dC_T}{dt} = kK_F^* C_L^{1/n} \tag{22}$$

Taking the derivative of Equation (21) with respect to time, it yields

$$\frac{dC_T}{dt} = \left[1 + \frac{WN_S^* K_F^*}{V}\frac{1}{n} C_L^{(1-n)/n}\right]\frac{dC_L}{dt} \tag{23}$$

Substituting Equation (23) into the left-hand side term of Equation (22), one obtains

$$-\frac{V}{WS_S}\left[1 + \frac{WN_S^* K_F^*}{V}\frac{1}{n} C_L^{1-n/n}\right]\frac{dC_L}{dt} = kK_F^* C_L^{1/n} \tag{24}$$

and, rearranging and separating the variables, the following differential equation is obtained:

$$-\frac{V}{WS_S}\frac{1}{kK_F^*}\frac{dC_L}{C_L^{1/n}} - \frac{1}{S_S}\frac{N_S^*}{kn}\frac{dC_L}{C_L} = dt \tag{25}$$

As done in the case of Langmuir adsorption isotherm, integration of Equation (25) is performed with the condition that at $t = 0$ the substrate concentration in the liquid phase is that in equilibrium with the initial photoadsorbed amount, $C_{L,0}$; this initial concentration is unknown, but it may be determined

by the regression analysis carried out with the experimental data obtained after the start of irradiation. The integration yields

$$\frac{V}{WS_S}\frac{1}{kK_F^*}\frac{n}{n-1}\left(C_{L,0}^{(n-1)/n}-C_L^{(n-1)/n}\right)+\frac{1}{S_S}\frac{N_S^*}{kn}\ln\frac{C_{L,0}}{C_L}=t \tag{26}$$

Equation (26) contains five unknown parameters, $K_F^*$, $N_S^*$, $n$, $k$, and $C_{L,0}$, whose determination may be carried out by a best fitting procedure.

## 4.3. Redlich–Peterson isotherm

Since in heterogenous catalysis most of the adsorbents follow Langmuir or Freundlich models, much better than Temkin model, an attempt is made here to test the photoadsorption validity with respect to Redlich–Peterson (R–P) model (Redlich and Peterson, 1959). The R–P isotherm model combines elements from both the Langmuir and the Freundlich equations and the mechanism of adsorption is a hybrid one and it does not follow ideal monolayer adsorption. The R–P isotherm is an empirical equation, designated the "three parameter equation," which may be used to represent adsorption equilibria over a wide concentration range (Ahmaruzzaman and Sharma, 2005; Allen et al., 2004; Kumar and Sivanesan, 2005; Matthews and Weber, 1976 ). The R–P adsorption isotherm is described by the following relationship:

$$\frac{n_S}{W}=\frac{K_{R-P}^*C_L}{1+\alpha_{R-P}^*C_L^{\beta}} \tag{27}$$

where $K_{R-P}^*$ and $\alpha_{R-P}^*$ are R–P isotherm constants which refer to the adsorption capacity and the surface energy, respectively. The exponent $\beta$ is the heterogeneity factor which lies between 1 and 0. The equation can be reduced to the Langmuir equation as $\beta$ approaches 1 while it becomes the Henry's law equation when $\beta=0$. By solving Equation (27) with respect to $n_S$ and substituting in Equation (6), the result is

$$C_T=C_L+\frac{W}{V}\frac{K_{R-P}^*C_L}{1+\alpha_{R-P}^*C_L^{\beta}} \tag{28}$$

In the cases of Langmuir and Freundlich isotherms, it has been assumed that the total disappearance rate of substrate per unit surface area, $r_T$, follows a pseudo-first-order kinetics with respect to the substrate concentration which is expressed by its fractional coverage. The same assumption is made for R–P isotherm; however, as the R–P isotherm relates an adsorbed amount (and not a fractional coverage) with the equilibrium concentration

in the liquid phase, the $r_T$ term is written as

$$r_T \equiv -\frac{V}{WS_S}\frac{dC_T}{dt} = kC_{Surface} = k\frac{n_S}{WS_S} \tag{29}$$

in which $C_{Surface}$ is the surface concentration of adsorbed species (adsorbed moles/catalyst surface area) (Minero and Vione, 2006). Substituting in Equation (29) the R–P relationship [Equation (27)] produces

$$-\frac{V}{W}\frac{dC_T}{dt} = k\frac{K^*_{R-P}C_L}{1+\alpha^*_{R-P}C_L^\beta} \tag{30}$$

Taking the derivative of Equation (28) with respect to time, it yields

$$\frac{dC_T}{dt} = \left[1+\frac{WK^*_{R-P}}{V}\frac{1+\alpha^*_{R-P}C_L^\beta(1-\beta K^*_{R-P})}{(1+\alpha^*_{R-P}C_L^\beta)^2}\right]\frac{dC_L}{dt} \tag{31}$$

Substituting Equation (31) in the left-hand side term of Equation (30), one obtains

$$-\frac{V}{W}\left[1+\frac{WK^*_{R-P}}{V}\frac{1+\alpha^*_{R-P}C_L^\beta(1-\beta K^*_{R-P})}{(1+\alpha^*_{R-P}C_L^\beta)^2}\right]\frac{dC_L}{dt} = k\frac{K^*_{R-P}C_L}{1+\alpha^*_{R-P}C_L^\beta} \tag{32}$$

and, rearranging and separating the variables, the following differential equation is obtained:

$$\begin{aligned}&-\frac{V}{WkK^*_{R-P}}\frac{dC_L}{C_L}-\frac{\alpha^*_{R-P}V}{WkK^*_{R-P}}C_L^{\beta-1}dC_L-\frac{1}{k}\frac{dC_L}{C_L(1+\alpha^*_{R-P}C_L^\beta)}\\&-\frac{V\alpha^*_{R-P}(1-\beta K^*_{R-P})}{WkK^*_{R-P}}\frac{C_L^{\beta-1}dC_L}{1+\alpha^*_{R-P}C_L^\beta} = dt\end{aligned} \tag{33}$$

As done in the case of previous adsorption isotherms, integration of Equation (33) is performed with the condition that at $t=0$ the substrate concentration in the liquid phase is that in equilibrium with the initial photoadsorbed amount, $C_{L,0}$; this initial concentration is unknown, but it may be determined by the regression analysis carried out with the experimental data obtained after the start of irradiation. The integration yields

$$\begin{aligned}&\frac{V}{WkK^*_{R-P}}\ln\left(\frac{C_{L,0}}{C_L}\right)+\frac{\alpha^*_{R-P}V}{Wk\beta K^*_{R-P}}(C_{L,0}^\beta-C_L^\beta)+\frac{1}{k\beta}\ln\left(\frac{1+\alpha^*_{R-P}C_L^\beta}{1+\alpha^*_{R-P}C_{L,0}^\beta}\frac{C_{L,0}^\beta}{C_L^\beta}\right)\\&+\frac{V(1-\beta K^*_{R-P})}{Wk\beta K^*_{R-P}}\ln\left(\frac{1+\alpha^*_{R-P}C_{L,0}^\beta}{1+\alpha^*_{R-P}C_L^\beta}\right) = t\end{aligned} \tag{34}$$

Equation (34) contains five unknown parameters, $K^*_{R-P}$, $\alpha^*_{R-P}$, $\beta$, $k$, and $C_{L,0}$, whose determination may be carried out by a best fitting procedure.

## 5. RESULTS

As expected, no photodegradation of benzyl alcohol or phenol was observed in oxygenated solution under irradiation but without catalyst. In the presence of catalyst but without irradiation no oxidation of benzyl alcohol or phenol was detected but a small adsorption of benzyl alcohol was measured while for phenol it was negligible.

The photoreactivity runs carried out by bubbling pure oxygen or air gave the same results so that it may be concluded that the oxygen concentration is not limiting the substrate degradation rate at the used experimental conditions.

Figures 3 and 4 report the photoreactivity results obtained from representative runs carried out at different initial benzyl alcohol concentrations and two lamp powers; for all of these runs, the same amount of catalyst was used.

In Figures 3–5, the concentration values reported for the zero time correspond to those of the starting solution, that is, without catalyst and irradiation. It must be reported that at the end of dark period (lasting 30 min) the benzyl alcohol concentration in the suspension is a little lesser than that of the starting solution. The calculations of photoadsorbed amount, however, have been performed by hypothesizing that all the molecules present on the catalyst surface participate in the

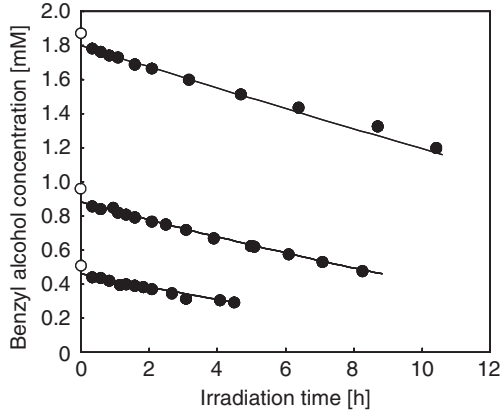


**Figure 3** Experimental values of benzyl alcohol concentration vs. irradiation time. Home-prepared catalyst amount: 0.4 g $L^{-1}$, lamp power, 125 W. The empty symbols indicate the concentration of starting solution. The solid lines represent the Langmuir photoadsorption model [Equation (19)] (Yurdakal et al., 2008b).

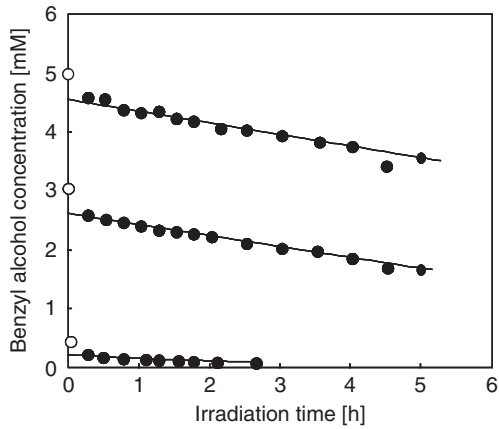


**Figure 4** Experimental values of benzyl alcohol concentration vs. irradiation time. Home-prepared catalyst amount: 0.4 g $L^{-1}$, lamp power, 500 W. The empty symbols indicate the concentration of starting solution. The solid lines represent the Langmuir photoadsorption model [Equation (19)] (Yurdakal et al., 2008b).

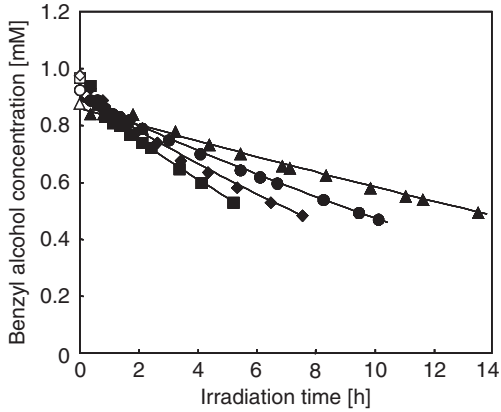


**Figure 5** Experimental values of benzyl alcohol concentration vs. irradiation time. Home prepared catalyst amount: (▲) 0.1 g $L^{-1}$; (•) 0.2 g $L^{-1}$; (□) 0.6 g $L^{-1}$; (■) 0.8 g $L^{-1}$. Lamp power, 125 W. The empty symbols indicate the concentration of starting solution. The solid lines represent the photoadsorption model [Equation (19)] (Yurdakal et al., 2008b).

photoprocess and therefore the concentration of the starting solution has been taken into account.

Benzaldehyde was the intermediate product detected in the course of benzyl alcohol photocatalytic oxidation, $CO_2$ being the other oxidation product. No other intermediates were detected in all the course of the runs indicating that at the used experimental conditions the produced

aldehyde does not compete with alcohol for photoadsorption and oxidation. This feature implies that the benzyl alcohol degradation kinetics did not change in the course of the runs due to the accumulation of intermediate products in the reaction ambient.

Figure 5 reports the results obtained from runs carried out with different amounts of catalyst; for all these runs the same initial benzyl alcohol concentration and lamp power were used.

Figures 6 and 7 report the photoreactivity results obtained from representative runs carried out at different initial phenol concentrations (with the same amount of catalyst) and at different amounts of catalyst (with the same initial phenol concentration), respectively.

In Figures 6 and 7, the phenol concentration values reported for the zero time correspond to those of the starting solution, that is, without catalyst and irradiation. It is useful to report that the adsorption of phenol in the dark is negligible so that the phenol concentration in the solution did not change after the addition of the catalyst.

In the course of phenol photocatalytic oxidation, the main products determined through TOC and HPLC analyses were $CO_2$ and hydroquinone and catechol, as expected having in mind that the photocatalytic oxidation of organic compounds on illuminated $TiO_2$ proceeds via $^{\bullet}OH$ attack on the substrate. The experimental results indicate that since the start of irradiation two parallel reaction pathways take place: direct mineralization of phenol to $CO_2$ (occurring through a series of reactions taking place over the catalyst surface and producing intermediates not desorbing to the bulk of solution) and partial oxidation to hydroxylated compounds (Salaices et al., 2004).

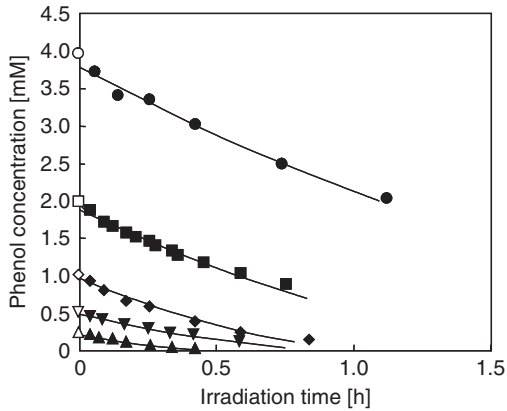


**Figure 6** Experimental values of phenol concentration vs. irradiation time. $TiO_2$ P25 catalyst amount: 0.32 g $L^{-1}$, lamp power, 500 W. The empty symbols indicate the concentration of starting solution. The solid lines represent the Freundlich photoadsorption model [Equation (26)].

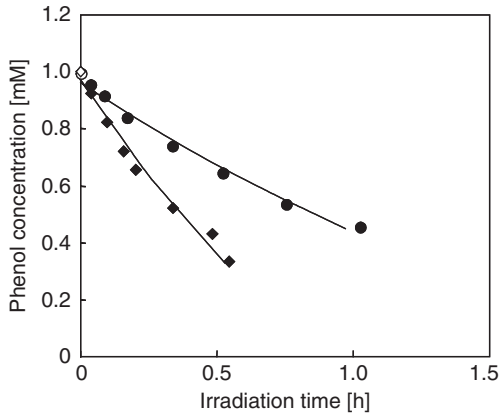


**Figure 7** Experimental values of phenol concentration vs. irradiation time. $TiO_2$ P25 catalyst amount: (•) 0.05 g $L^{-1}$ and (◆) 0.64 g $L^{-1}$. Lamp power, 500 W. The empty symbols indicate the concentration of starting solution. The solid lines represent the Freundlich photoadsorption model [Equation (26)].

The carbon balance between reacted phenol and produced $CO_2$ and dihydroxylated compounds was satisfactory ($> 98\%$) for phenol conversion less than 60%. On this basis it may be assumed that at the used experimental conditions the stable intermediate products of phenol photodegradation do not compete with phenol for photoadsorption and oxidation, at least in the time needed for 60% conversion.

This feature implies that the phenol degradation kinetics did not change in the course of the runs due to the accumulation of intermediate products in the reaction ambient. As a consequence, only the phenol concentration values relative to conversion below 60% have been taken into account in the course of photoadsorption modeling.

## 6. DISCUSSION

Nonlinear optimization techniques have been applied to determine isotherm parameters. It is well known (Ncibi, 2008) that the use of linear expressions, obtained by transformation of nonlinear one, distorts the experimental error by creating an inherent error estimation problem. In fact, the linear analysis method assumes that (i) the scatter of points follows a Gaussian distribution and (ii) the error distribution is the same at every value of the equilibrium liquid-phase concentration. Such behavior is not exhibited by equilibrium isotherm models since they have nonlinear shape; for this reason the error distribution gets altered after transforming the data

to linear. Nonlinear regression method avoids such errors, making this analyzing technique the most appropriate to obtain more realistic isotherm parameters.

In this work, among different error functions the MPSD was used to enable the optimization process to determine and evaluate the fit of the isotherm equation to the experimental data. This error function is similar to a geometric mean error distribution which is modified to allow for the number of degrees of freedom of the system. For each case the isotherm parameters were determined by minimizing the MPSD function across the liquid-phase concentration range using the Data-Plot solver (Heckert and Filliben, 2003a, b). It was assumed that both the liquid-phase and the solid-phase concentrations contribute equally to weighting the error criterion chosen for the model solution procedure.

## 6.1. Benzyl alcohol photoadsorption

The fitting of the Langmuir, Freundlich, and R–P models to the data has been firstly applied to the photoreactivity results obtained from runs carried out at equal mass of catalyst and lamp power. For the Langmuir model, the following procedure has been followed. In order to have an estimate of parameters values, the data at high initial concentration of benzyl alcohol have been fitted to Equation (A6) (see Appendix A1) and those at low initial concentration to Equation (A13). The parameters obtained by these fitting procedures have been used to determine $K_L^*$ and $N_S^*$ by means of Equation (A18). As inequalities A1 and A7 were not strongly satisfied, the fitting procedure has been repeated by using the general equation of the proposed model [Equation (19)].

For the runs carried out at different catalyst amounts, the general equations for the liquid concentration profile [Equations (19), (26), and (34)] have been used. For Freundlich and Redlich–Peterson isotherms, the fitting obtained for each run was quite satisfactory ($R^2 > 0.98$); however, for the runs carried out at equal amount of catalyst, the Freundlich and Redlich–Peterson parameter values showed a dependence on initial benzyl alcohol concentration; on the contrary, same values were obtained for Langmuir parameters. On this basis the Langmuir isotherm seems to best describe the photoadsorption phenomenon of benzyl alcohol on home-prepared $TiO_2$ catalyst. The continuous lines drawn through the data of Figures 3–5 represent Equation (19), and a very satisfactory fitting ($R^2 > 0.99$) may be noted. The values of kinetic and Langmuir parameters ($k$, $K_L^*$, and $N_S^*$), obtained by the best fitting procedure, are reported later (see Figure 10).

The suitability of Langmuir model to describe the photoadsorption phenomenon has been further checked by using the linear form of Langmuir equation [Equation (A18)]. Figure 8 reports the values of the $C_{L,0}/(C_{T,0} - C_{L,0})$

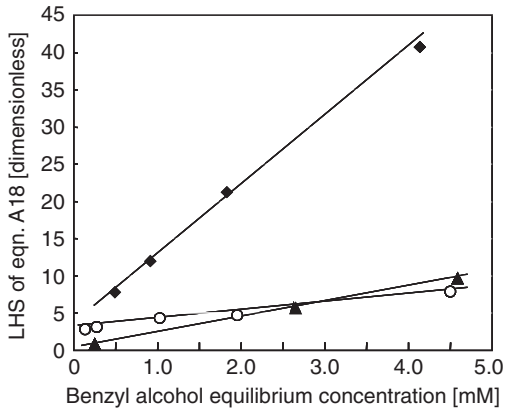


**Figure 8** Linear form of Langmuir model. The left-hand side of Equation (A18), $C_{L,0}/(C_{T,0} - C_{L,0})$, vs. $C_{L,0}$ for runs carried out under irradiation with lamp power of 125 W (◆), 500 W (▲), and in the dark (○). The dark data are multiplied for $10^{-3}$. The solid lines represent the Langmuir photoadsorption model [Equation (A18)] (Yurdakal et al., 2008b).

group obtained from runs carried out at equal mass of catalyst and lamp power vs. the benzyl alcohol equilibrium concentration. The straight lines drawn through the data represent Equation (A18), and a very good fitting ($R^2 > 0.99$) may be noted.

The slopes and linear coefficients of lines allow to determine the $N_S^*$ and $K_L^*$ values corresponding to these runs; these values are almost the same as those determined by means of Equation (19) (error percentage, $\pm 4\%$). Figure 8 also reports the adsorption results obtained in the absence of irradiation, that is, in the dark. A least-squares best fitting procedure allows to determine the values ($R^2 > 0.99$) of the Langmuir equilibrium constant and the maximum adsorption capacity in the absence of irradiation, that is, $K_L = 350\ M^{-1}$ and $N_S = 4.57 \times 10^{-6}$ mol/g of catalyst.

The effect of catalyst amount on photoadsorption capacity is shown in Figure 9. This figure reports the benzyl alcohol moles photoadsorbed per unit mass of catalyst vs. the catalyst amount; the reported data refer to runs carried out at equal initial benzyl alcohol concentration and lamp power. From the observation of data of Figure 9, a decrease of specific photoadsorption capacity by increasing the catalyst amount, differently from that expected on thermodynamic basis for which an increase of catalyst amount determines a corresponding increase of adsorbed substrate, may be noted.

This finding may be explained by considering that an increase of catalyst amount determines an increase of photons absorbed by the suspension but the photon flow absorbed *by the unit mass of catalyst* decreases. As photoadsorption is likely to be strongly dependent on absorbed photon flow, the increase of catalyst amount is eventually detrimental for specific photoadsorption.

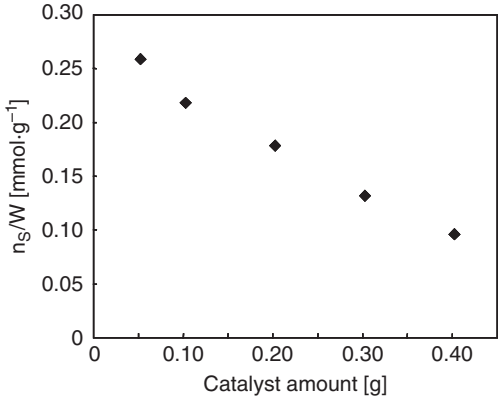


**Figure 9** Photoadsorbed amount of benzyl alcohol per unit mass of catalyst, $n_S/W$, vs. the mass of catalyst. Initial benzyl alcohol concentration, 1 mM, lamp power, 125 W (Yurdakal et al., 2008b).

The consideration that the photon flow absorbed by the unit mass of catalyst is the parameter mainly affecting the photoadsorption phenomenon is strengthened by the results reported in Figure 10. This figure reports the values of the model parameters, $K_L^*$, $N_S^*$, and $k$, vs. the absorbed photon flow per unit mass of catalyst. The $K_L$ and $N_S$ values obtained from dark experiments are also reported. It may be noted that all parameters increase by increasing the specific photon absorption. While it is known that in thermal catalysis a temperature

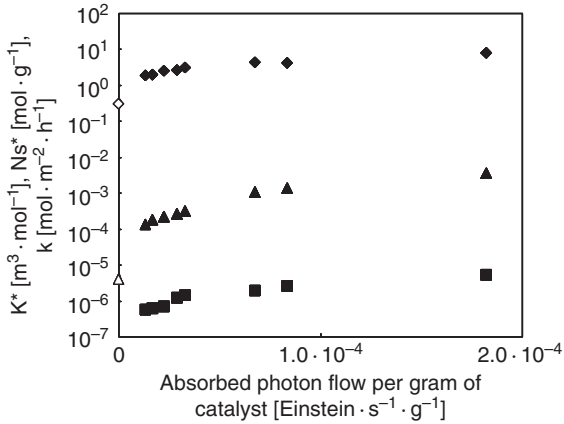


**Figure 10** Values of kinetic and Langmuir model parameters [see Equation (19)] vs. the absorbed photon flow per unit mass of catalyst. ◆, $K_L^*$; ▲, $N_S^*$; ■, $k$. The empty symbols refer to dark conditions (Yurdakal et al., 2008b).

increase determines an increase of kinetic and equilibrium adsorption constants, the results of Figure 10 also show a beneficial effect of absorbed photons on the photoadsorbed amount of solute. This effect is very noticeable if a comparison is done between irradiated and dark conditions. The values of $K_L^*$ and $N_S^*$ are one and two orders of magnitude, respectively, higher than those obtained in the absence of irradiation.

## 6.2. Phenol photoadsorption

The fitting of photoreactivity data obtained from runs carried out at equal mass of catalyst and at different catalyst amounts has been carried out by applying the general equations of Langmuir, Freundlich, and Redlich–Peterson isotherms [Equations (19), (26), and (34)]. For Langmuir and Redlich–Peterson isotherms, the fitting obtained for each run was quite satisfactory ($R^2 > 0.98$); however, for the runs carried out at equal amount of catalyst, the Langmuir and Redlich–Peterson parameters values showed a dependence on initial phenol concentration; on the contrary, same values were obtained for Freundlich parameters. On this basis the Freundlich isotherm seems to best describe the photoadsorption phenomenon of phenol on commercial $TiO_2$ catalyst (Degussa P25). The continuous lines drawn through the data of Figures 6 and 7 represent Equation (26) with $n = 2$, and a satisfactory fitting ($R^2 > 0.98$) may be noted.

The suitability of Freundlich model to describe the photoadsorption phenomenon has been further checked by using the Freundlich equation [Equation (20)] in its linear form. Figure 11 reports the values of the $n_S/W$ group obtained from runs carried out at equal mass of catalyst vs. the square

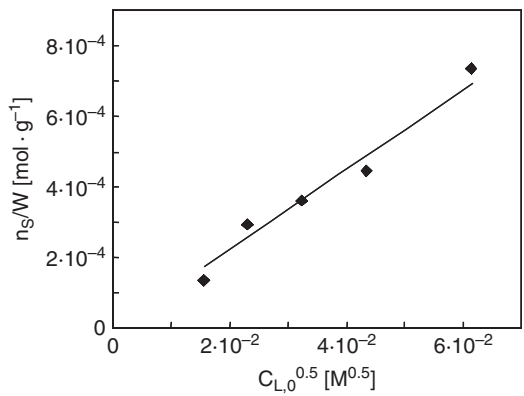


**Figure 11** Linear form of Freundlich model. The left-hand side of Equation (19), $n_S/W$, vs. $C_{L,0}^{0.5}$ for runs carried out under irradiation with lamp power of 500 W. The solid line represents the Freundlich photoadsorption model [Equation (20)].

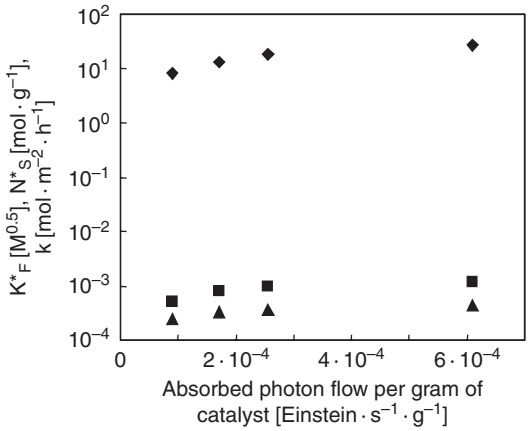


**Figure 12** Values of kinetic and Freundlich model parameters [see Equation (26)] vs. the absorbed photon flow per unit mass of catalyst. ◆, $K^*_F$; ▲, $N^*_S$; ■, $k$.

root of phenol equilibrium concentration. The straight line drawn through the data represents Equation (20); the slope value of this line, equal to the $(K^*_F * N^*_S)$ product, is 0.0112, very near to the 0.0107 value obtained from the best fitting procedure.

The values of kinetic and Freundlich parameters (k, $K^*_F$, and $N^*_S$), obtained from runs carried out with different amounts of catalyst, are reported in Figure 12 vs. the absorbed photon flow per unit mass of catalyst. These values show the same feature of Langmuir parameters obtained for benzyl alcohol oxidation, that is, they decrease by decreasing the photon flow absorbed *by the unit mass of catalyst*. As in the case of benzyl alcohol, the consideration that the photon flow absorbed by the unit mass of catalyst is the parameter mainly affecting the photoadsorption phenomenon is strengthened by the results reported in Figure 12.

## 6.3. Reaction mechanism

According to the preceding discussion, the primary events occurring at the photocatalyst surface may be described by the following mechanism: The primary photochemical act, following the light absorption by the semiconductor, is the generation of electron/hole pairs. The light absorbed by the unit surface of catalyst and unit time produces equivalent bulk concentrations of charge carriers, $e^-$ and $h^+$:

$$\textit{Charge separation} \quad TiO_2 + h\nu \rightarrow e^- + h^+ \tag{35}$$

The charge carriers can recombine either in the bulk or in the surface:

$$\textit{Bulk or surface recombination} \quad e^- + h^+ \rightarrow \text{heat, light} \tag{36}$$

or migrate to the surface where they are trapped by suitable electron and hole traps forming the corresponding active centers:

$$\textit{Electron trap} \quad S_e + e^- \rightarrow S_e^* \tag{37}$$

$$\textit{Hole trap} \quad S_h + h^+ \rightarrow S_h^* \tag{38}$$

If electron acceptors ($Ox_2$, like oxygen) or electron donors ($Red_1$, as organic substrates) are present at the surface, they can be photoadsorbed on the active centers:

$$\textit{Photoadsorption on } S_e^* \quad S_e^* + Ox_2 \rightarrow Ox_{2(\text{photoads})} \tag{39}$$

$$\textit{Photoadsorption on } S_h^* \quad S_h^* + Red_1 \rightarrow Red_{1(\text{photoads})} \tag{40}$$

The photoadsorption steps are followed by oxidation of the organic substrate:

$$\textit{Oxidation} \quad Red_{1(\text{photoads})} + h^+ \rightarrow Ox_1^{\bullet} \tag{41}$$

and by reduction of the oxidant species:

$$\textit{Reduction} \quad Ox_{2(\text{photoads})} + e^- \rightarrow Red_2^{\bullet} \tag{42}$$

Competitive with reactions (37–40) are the back reactions:

$$\textit{Decay of } S_e^* \textit{ active center} \quad S_e^* \rightarrow S_e + e^- \tag{43}$$

$$\textit{Decay of } S_h^* \textit{ active center} \quad S_h^* \rightarrow S_h + h^+ \tag{44}$$

$$\textit{Photodesorption from } S_e^* \quad Ox_{2(\text{photoads})} \rightarrow S_e^* + Ox_2 \tag{45}$$

$$\textit{Photodesorption from } S_h^* \quad Red_{1(\text{photoads})} \rightarrow S_h^* + Red_1 \tag{46}$$

The combined reactions (35) and (36) or (37), (38), (43) and (44) or (39), (40), (45), and (46) yield a net cycle, where there is no use of the absorbed photons.

The radicals formed through reactions 41 and 42 may be further transformed by subsequent reaction with photogenerated active species or through reaction with solvent, other species present in solution (such

as $O_2$, $H_2O_2$, $O_2^-$), elimination of molecular groups or ions (Calza et al., 1997; Piccinini et al., 1997), or dimerization (Minero et al., 1995). The additional transformations may lead to the complete degradation of the organic compound to $CO_2$ and inorganic anions. In addition to all the preceding reactions, which hold for a substrate that can only be oxidized, there are possible concurrent oxidative and reductive reactions, as observed for halomethanes degradation (Calza et al., 1997).

## 7. CONCLUSIONS

The method here proposed for the determination of photoadsorption capacity under reaction conditions gives valuable information on the influence of absorbed photons on kinetics and thermodynamics of a photocatalytic reaction. The consideration that the photon flow absorbed by the unit mass of catalyst is the parameter mainly affecting the photoadsorption phenomenon is strengthened by all the results. Under irradiation, the catalyst surface undergoes noticeable changes (for example, from hydrophobic to hydrophilic character), these changes depending on photon absorption. The photoadsorbed amount of solute shows firstly a sharp increase with absorbed photons, this increase being less important at high photon absorption. This behavior appears to indicate that the number of photoactive sites increases with photon absorption until a value is reached for which an increase of absorbed photon does not affect the amount of photoadsorbed substrate. This limiting amount should be characteristic of the catalyst surface and the physicochemical features of solute and medium (pH, ionic strength, etc.).

The basic assumptions of model are that (i) the $TiO_2$ surface, once firstly irradiated, needs a certain time to reach a thermodynamic equilibrium with the surrounding medium and (ii) photoadsorption is fast with respect to the reaction. The best fitting procedure suggests that the Langmuir isotherm is the most suitable one for describing benzyl alcohol photoadsorption while the Freundlich isotherm better describes phenol photoadsorption. In both cases the other tested isotherms (Freundlich and Redlich–Peterson ones for benzyl alcohol and Langmuir and Redlich–Peterson ones for phenol) did not give a satisfactory fitting. It must be outlined, however, that it is likely that the chemical features of solute determine the most suitable isotherm for modeling the photoadsorption phenomenon.

The modeling results indicate that the parameters of the Langmuir and Freundlich models depend on the absorbed photon flow. In order to take into account the dependence on photon flows, it would be necessary to develop a kinetic model based on the proposed reaction mechanism in which the photons appear as reactants. Work on this field is in progress.

# APPENDICES

## A1. ASYMPTOTIC CASES OF LANGMUIR PHOTOADSORPTION ISOTHERM

A straightforward determination of $K_L^*$, $N_S^*$, $k$, and $C_{L,0}$ parameters can be done in the following way. $k$ and $C_{L,0}$ may be easily determined by considering two asymptotic situations of Langmuir adsorption isotherm, that is, very high or very low substrate concentration. At very high concentrations of substrate the following inequality may be assumed to hold:

$$K_L^* C_L >> 1 \tag{A1}$$

In this case from Equation (13) one obtains

$$\theta_{Sub} \equiv \frac{n_S}{WN_S^*} = \frac{K_L^* C_L}{1 + K_L^* C_L} \approx 1 \tag{A2}$$

and Equation (14) transforms in

$$C_T = C_L + \frac{WN_S^*}{V} \tag{A3}$$

The total disappearance rate of substrate per unit surface area, $r_T$, gets of zero order so that Equation (15) can be written as:

$$-\frac{V}{WS_S}\frac{dC_T}{dt} = k \tag{A4}$$

Taking the derivative of Equation (A3) with respect to time, it yields that $dC_T/dt = dC_L/dt$. Substituting this equality in Equation (A4) and rearranging, one obtains

$$-\frac{dC_L}{dt} = \frac{WS_S}{V}k \tag{A5}$$

Integration of Equation (A5) with the condition that $C_L = C_{L,0}$ for $t = 0$ yields the following relationship:

$$C_L = C_{L,0} - \frac{WS_S}{V}kt \tag{A6}$$

which is a linear relationship between the concentration values measured in the solution and the irradiation time. The intercept and slope values allow to determine the $C_{L,0}$ and $k$ values.

At very low concentrations of substrate, the following inequality may be assumed to hold:

$$K^*_{\mathrm{L}} C_{\mathrm{L}} \ll 1 \tag{A7}$$

In this case from Equation (13) one obtains

$$\theta_{\mathrm{Sub}} \equiv \frac{n_{\mathrm{S}}}{WN^*_{\mathrm{S}}} = \frac{K^*_{\mathrm{L}} C_{\mathrm{L}}}{1 + K^*_{\mathrm{L}} C_{\mathrm{L}}} \approx K^*_{\mathrm{L}} C_{\mathrm{L}} \tag{A8}$$

and from Equation (14) one obtains

$$C_{\mathrm{T}} = C_{\mathrm{L}} + \frac{WN^*_{\mathrm{S}} K^*_{\mathrm{L}}}{V} C_{\mathrm{L}} \tag{A9}$$

The total disappearance rate of substrate per unit surface area, $r_{\mathrm{T}}$, turns of first order with respect to the substrate concentration and Equation (15) can be written as

$$-\frac{V}{WS_{\mathrm{S}}} \frac{\mathrm{d}C_{\mathrm{T}}}{\mathrm{d}t} = kK^*_{\mathrm{L}} C_{\mathrm{L}} \tag{A10}$$

Taking the derivative of Equation (A9) with respect to time, it yields

$$\frac{\mathrm{d}C_{\mathrm{T}}}{\mathrm{d}t} = \left(1 + \frac{WN^*_{\mathrm{S}} K_{\mathrm{L}}{}^*}{V}\right) \frac{\mathrm{d}C_{\mathrm{L}}}{\mathrm{d}t} \tag{A11}$$

Substituting this equality in Equation (A10) and rearranging, one obtains

$$-\frac{\mathrm{d}C_{\mathrm{L}}}{\mathrm{d}t} = \frac{WS_{\mathrm{S}} k K^*_{\mathrm{L}}}{V + N^*_{\mathrm{S}} K^*_{\mathrm{L}}} C_{\mathrm{L}} \tag{A12}$$

By integrating with the condition that $C_{\mathrm{L}} = C_{\mathrm{L},0}$ for $t = 0$, one obtains

$$\ln C_{\mathrm{L}} = \ln C_{\mathrm{L},0} - \frac{WS_{\mathrm{S}} k K^*_{\mathrm{L}}}{V + WN^*_{\mathrm{S}} K^*_{\mathrm{L}}} t \tag{A13}$$

which is a linear relationship in a semilogarithmic plot of concentration values vs. the irradiation time. The intercept value allows to determine the $C_{\mathrm{L},0}$ value while the slope contains two parameters, $K^*_{\mathrm{L}}$ and $N^*_{\mathrm{S}}$, that may be determined in the following way:

From the photoreactivity runs for which the inequalities (A1) and (A7) hold, the values of $C_{\mathrm{L},0}$ may be determined. Applying to the substrate the molar balance expressed by Equation (6) at the start of irradiation, that is, the zero time, yields

$$C_{\mathrm{T},0} = C_{\mathrm{L},0} + \frac{n_{\mathrm{S},0}}{V} \tag{A14}$$

in which $C_{\mathrm{T},0}$ is the total concentration of substrate and coincides with the concentration of initial solution and $n_{\mathrm{S},0}$ is the number of photoadsorbed

moles in equilibrium with the solution at $C_{L,0}$ concentration. In the statement of Equation (A14), it is assumed that only photoadsorption can occur on the surface of irradiated particles of catalyst and that the whole particles are irradiated. Equation (A14) allows to determine the $n_{S,0}$ value corresponding to a certain $C_{L,0}$:

$$n_{S,0} = V(C_{T,0} - C_{L,0}) \tag{A15}$$

All the $n_{S,0} - C_{L,0}$ couples of values are related by the Langmuir model [Equation (13)]:

$$\frac{n_{S,0}}{WN_S^*} = \frac{K_L^* C_{L,0}}{1 + K_L^* C_{L,0}} \tag{A16}$$

Inverting the terms of Equation (A16) and rearranging, one has

$$\frac{1}{n_{S,0}} = \frac{1}{WN_S^* K_L^* C_{L,0}} + \frac{1}{WN_S^*} \tag{A17}$$

Introducing Equation (A15) into Equation (A17) and multiplying Equation (A17) by $C_{L,0}$ yield Equation (A18), which is the linear form of Equation (A16):

$$\frac{C_{L,0}}{C_{T,0} - C_{L,0}} = \frac{V}{WN_S^* K_L^*} + \frac{V}{WN_S^*} C_{L,0} \tag{A18}$$

where $C_{L,0}/(C_{T,0} - C_{L,0})$ is a dependent variable, $C_{L,0}$ an independent variable, $V/(WK_L^* N_S^*)$ the linear coefficient, and $V/(WN_S^*)$ the angular coefficient of the straight line. Thus, by plotting $C_{L,0}/(C_{T,0} - C_{L,0})$ vs. $C_{L,0}$ one can determine the maximum adsorption capacity, $N_S^*$, and photoadsorption equilibrium constant, $K_L^*$, respectively, through the slope and linear coefficient of the straight line.

The determination of the value of $K_L^*$ allows checking the inequalities expressed by Equations (A1) and (A7). For the runs for which the previous inequalities do not hold, Equation (19) must be used for determining the only unknown parameter contained in it, that is, the $C_{L,0}$ value.

## A2. TEMKIN ISOTHERM

The Temkin isotherm model assumes that the heat of adsorption of all the molecules in the layer decreases linearly with coverage due to adsorbent–adsorbate interactions, and that the adsorption is characterized by a uniform distribution of the binding energies, up to some maximum

binding energy. By applying the Langmuir adsorption isotherm to this distribution of energies, the Temkin isotherm equation is derived (Satterfield, 1980):

$$\theta_{\mathrm{Sub}} \equiv \frac{n_{\mathrm{S}}}{WN_{\mathrm{S}}^{*}} = \frac{1}{f}\ln\left(K_{\mathrm{T}}^{*}C_{\mathrm{L}}\right) \tag{A19}$$

where $f$ is a constant related to the differential heat of adsorption at zero surface coverage, and $K_{\mathrm{T}}^{*}$ the Temkin equilibrium adsorption constant. By solving Equation (A19) with respect to $n_{\mathrm{S}}$ and substituting in Equation (6), the result is

$$C_{\mathrm{T}} = C_{\mathrm{L}} + \frac{WN_{\mathrm{S}}^{*}}{V}\frac{1}{f}\ln\left(K_{\mathrm{T}}^{*}C_{\mathrm{L}}\right) \tag{A20}$$

Substituting in Equation (11), the Temkin relationship (Equation (A19)) produces

$$-\frac{V}{WS_{\mathrm{S}}}\frac{\mathrm{d}C_{\mathrm{T}}}{\mathrm{d}t} = k\frac{1}{f}\ln\left(K_{\mathrm{T}}^{*}C_{\mathrm{L}}\right) \tag{A21}$$

Taking the derivative of Equation (A20) with respect to time, it yields

$$\frac{\mathrm{d}C_{\mathrm{T}}}{\mathrm{d}t} = \left[1 + \frac{WN_{\mathrm{S}}^{*}}{V}\frac{1}{f}\frac{1}{C_{\mathrm{L}}}\right]\frac{\mathrm{d}C_{\mathrm{L}}}{\mathrm{d}t} \tag{A22}$$

Substituting Equation (A22) in the left-hand side term of Equation (A21), one obtains

$$-\frac{V}{WS_{\mathrm{S}}}\left[1 + \frac{WN_{\mathrm{S}}^{*}}{V}\frac{1}{f}\frac{1}{C_{\mathrm{L}}}\right]\frac{\mathrm{d}C_{\mathrm{L}}}{\mathrm{d}t} = k\frac{1}{f}\ln\left(K_{\mathrm{T}}^{*}C_{\mathrm{L}}\right) \tag{A23}$$

and, rearranging and separating the variables, the following differential equation is obtained:

$$-\frac{V}{WS_{\mathrm{S}}}\frac{f}{k}\frac{\mathrm{d}C_{\mathrm{L}}}{\ln(K_{\mathrm{T}}^{*}C_{\mathrm{L}})} - \frac{N_{\mathrm{S}}^{*}}{S_{\mathrm{S}}}\frac{1}{k}\frac{\mathrm{d}C_{\mathrm{L}}}{C_{\mathrm{L}}\ln(K_{\mathrm{T}}^{*}C_{\mathrm{L}})} = \mathrm{d}t \tag{A24}$$

Equation (A24) contains five unknown parameters, $K_{\mathrm{T}}^{*}$, $N_{\mathrm{S}}^{*}$, $k$, $f$, and $C_{\mathrm{L},0}$, whose determination may be carried out by a best fitting procedure. As done in the cases previously described, integration of Equation (A24) must be performed with the condition that at $t = 0$ the substrate concentration in the liquid phase is that in equilibrium with the initial photoadsorbed amount, $C_{\mathrm{L},0}$; this initial concentration is unknown, but it may be determined by the regression analysis carried out with the experimental data obtained after the start of irradiation.

## LIST OF SYMBOLS

| | |
|---|---|
| $C_L$ | concentration in the liquid phase (M) |
| $C_{L,0}$ | substrate initial concentration in photoadsorption equilibrium (M) |
| $C_T$ | total concentration of the species (M) |
| $f$ | Temkin constant (dimensionless) |
| $h$ | Planck's constant ($6.626 \times 10^{-34}$ J·s) |
| $k$ | pseudo-first-order rate constant (mol $m^{-2}$ $h^{-1}$) |
| $k''$ | second-order rate constant (mol $m^{-2}$ $h^{-1}$) |
| $K_F^*$ | Freundlich isotherm constant ($M^n$) |
| $K_L^*$ | Langmuir photoadsorption equilibrium constant ($M^{-1}$) |
| $K_{R-P}^*$ | Redlich–Peterson isotherm constant ($dm^3 \cdot g^{-1}$) |
| $K_T^*$ | Temkin equilibrium adsorption constant ($M^{-1}$) |
| $n$ | Freundlich parameter (dimensionless) |
| $n_L$ | number of moles in the fluid phase (moles) |
| $n_S$ | number of moles photoadsorbed on the solid phase (moles) |
| $N_S^*$ | maximum capacity of photoadsorbed moles of substrate (mol $g^{-1}$) |
| $n_{S,Ox}$ | oxygen moles photoadsorbed on the solid (moles) |
| $N_{S,Ox}^*$ | maximum capacity of photoadsorbed moles of oxygen (mol $g^{-1}$) |
| $n_T$ | total number of moles present in the photoreactor (moles) |
| $r_T$ | total disappearance rate of substrate per unit surface area (mol $m^{-2}$ $h^{-1}$) |
| $S$ | catalyst surface area ($m^2$) |
| $S_S$ | catalyst specific surface area ($m^2$ $g^{-1}$) |
| $t$ | time (h) |
| $V$ | volume of the liquid phase ($dm^3$) |
| $W$ | mass of catalyst (g) |
| $\alpha_{R-P}^*$ | Redlich–Peterson isotherm constant ($M^{-\beta}$) |
| $\beta$ | Redlich–Peterson heterogeneity factor (dimensionless) |
| $v$ | radiation wavenumber ($nm^{-1}$) |
| $\theta_{Ox}$ | oxygen fractional coverage of the surface (dimensionless) |
| $\theta_{Sub}$ | substrate fractional coverage of the surface (dimensionless) |

## REFERENCES

Addamo, M., Augugliaro, V., Di Paola, A., García-López, E., Loddo, V., Marcì, G., Molinari, R., Palmisano, L., and Schiavello, M. *J. Phys. Chem. B* **108**, 3303 (2004).

Ahmaruzzaman, M., and Sharma, D.K. *J. Colloid Interface Sci.* **287**, 14 (2005).

Allen, S.J., Mckay, G., and Porter, J.F. *J. Colloid Interface Sci.* **280**, 322 (2004).

Asakuma, N., Fukui, T., Toki, M., Awazu, K., and Imai, H. *Thin Solid Films* **445**, 284 (2003).

Augugliaro, V., Litter, M., Palmisano, L., and Soria, J. *J. Photochem. Photobiol. C* **7**, 127 (2006).

Bickley, R.I. "Fundamental Aspects of the Adsorption and the Desorption of Gases at SolidSurfaces under Illumination" *in* M. Schiavello (Ed.), "Photoelectrochemistry,

Photocatalysis and Photoreactors, Fundamentals and Developments". Reidel, Dordrecht (1985a), pp. 379–388.
Bickley, R.I. "Some Experimental Investigations of Photosorption Phenomena at the Gas-Solid Interface" *in* M. Schiavello (Ed.), "Photoelectrochemistry, Photocatalysis and Photoreactors, Fundamentals and Developments". Reidel, Dordrecht (1985b), pp. 491–502.
Bickley, R.I. "Photoadsorption and Photodesorption at the Gas-Solid Interface Part I Fundamental Concepts" *in* M. Schiavello (Ed.) "Photocatalysis and Environment Trends and Applications". Kluwer, Dordrecht (1988a), pp. 223–232.
Bickley, R.I. "Photoadsorption and Photodesorption at the Gas-Solid Interface Part II Photoelectronic Effects Relating to Photochromic Changes and to Photosorption" *in* M. Schiavello (Ed.), "Photocatalysis and Environment Trends and Applications". Kluwer, Dordrecht (1988b), pp. 233–239.
Braslavsky, S.E. *Pure Appl. Chem.* **79**, 293 (2007).
Calza, P., Minero, C., and Pelizzetti, E. *Environ. Sci. Technol.* **31**, 2198 (1997).
Carp, O., Huisman, C.L., and Reller, A. *Prog. Solid State Chem.* **32**, 33 (2004).
de Lasa, H., Serrano, B., and Salaices, M. "Photocatalytic Reaction Engineering". Springer, New York (2005).
Demeestere, K., De Visscher, A., Dewulf, J., Van Leeuwen, M., and Van Langenhove, H. *Appl. Catal. B* **54**, 261 (2004).
Fujishima, A., and Honda, K. *Nature* **238**, 37 (1972).
Fujishima, A., Hashimoto, K., and Watanabe, T. "$TiO_2$ Photocatalysis: Fundamentals and Applications". Bkc Inc., , Tokyo (1999).
Fujishima, A., Rao, T.N., and Tryk, D.A. *J. Photochem. Photobiol. C* **1**, 1 (2000).
Fujishima, A., and Zhang, X. *Crit. Rev. Chim.* **9**, 7 (2006).
Gonzalez, M.A., Howell, S.G., and Sikdar, S.K. *J. Catal.* **183**, 159 (1999).
Gora, A., Toepfer, B., Puddu, V., and Li Puma, G. *Appl. Catal. B* **65**, 1 (2006).
Heckert, N.A., and Filliben, J.J. "NIST Handbook 148: DATAPLOT Reference Manual, Volume I: Commands". National Institute of Standards and Technology Handbook Series, Gaithersburg (2003a).
Heckert, N.A., and Filliben, J.J. "NIST Handbook 148: Dataplot Reference Manual, Volume II: Let Subcommands and Library Functions". National Institute of Standards and Technology Handbook Series, Gaithersburg (2003b).
Hoffmann, M.R., Martin, S.T., Choi, W.Y., and Bahnemann, D.W. *Chem. Rev.* **95**, 69 (1995).
Ibrahim, H., and De Lasa, H. *AIChE J.* **50**, 1017 (2004).
Ignatchenko, A., Nealon, D.G., Dushane, R., and Humphries, K. *J. Mol. Cat. A* **256**, 57 (2006).
Kaneko, M., and Okura, I. (Eds.), "Photocatalysis: Science and Technology". Springer-Verlag, Heildelberg, New York (2002).
Krýsa, J., Waldner, G., Měšťánková, H., Jirkovský, J., and Grabner, G. *Appl. Catal. B* **64**, 290 (2006).
Kumar, K.V., and Sivanesan, S. *J. Hazard. Mater.* **126**, 198 (2005).
Lee, Y.C., Hong, Y.P., Lee, H.Y., Kim, H., Jung, Y.J., Ko, K.H., Jung, H.S., and Hong, K.S. *J. Colloid Interface Sci.* **267**, 127 (2003).
Linsebigler, A.L., Lu, G.G., and Yates, J.T. *Chem. Rev.* **95**, 735 (1995).
Matthews, A.P., and Weber Jr., W.J. *AIChE Symp. Ser.* **73**, 91 (1976).
Meriaudeau, P., and Vedrine, J.C. *J. Chem. Soc. Faraday Trans. II* **72**, 472 (1976).
Mills, A., and Le Hunte, S. *J. Photochem. Photobiol. A* **108**, 1 (1997).
Minero, C., Pelizzetti, E., Pichat, P., Sega, M., and Vincenti, M. *Environ. Sci. Technol.* **29**, 2226 (1995).
Minero, C., and Vione, D. *Appl. Catal. B* **67**, 257 (2006).
Miyauchi, M., Kieda, N., Hishita, S., Mitsuhashi, T., Nakajima, A., Watanabe, T., and Hashimoto, K. *Surf. Sci.* **511**, 401 (2002).
Mohamed, O.S., Gaber, A.E.M., and Abdel-Wahab, A.A. *J. Photochem. Photobiol. A* **148**, 205 (2002).

Mori, K., Imaoka, S., Nishio, S., Nishiyama, Y., Nishiyama, N., and Yamashita, H. *Microporous Mesoporous Mater.* **101**, 288 (2007).
Murphy, W.R., Veerkamp, T.H., and Leland, T.W. *J. Catal.* **43**, 304 (1976).
Murzin, D.Y., and Salmi, T. "Catalytic Kinetics". Elsevier, Amsterdam (2005).
Nakajima, A., Koizumi, S., Watanabe, T., and Hashimoto, K. *J. Photochem. Photobiol. A* **146**, 129 (2001).
Ncibi, M.C. *J. Hazard. Mater.* **153**, 207 (2008).
Palmisano, G., Addamo, M., Augugliaro, V., Caronna, T., Di Paola, A., García-López, E., Loddo, V., Marcì, G., Palmisano, L., and Schiavello, M. *Catal. Today* **122**, 118 (2007b).
Palmisano, G., Loddo, V., Yurdakal, S., Augugliaro, V., and Palmisano, L. *AIChE J.* **53**, 961 (2007c).
Palmisano, G., Yurdakal, S., Augugliaro, V., Loddo, V., and Palmisano, L. *Adv. Synth. Catal*. **349**, 964 (2007a).
Piccinini, P., Minero, C., Vincenti, M., and Pelizzetti, E. *J. Chem. Soc. Faraday Trans.* **93**, 1993 (1997).
Redlich, O., and Peterson, D.L. *J. Phys. Chem.* **63**, 1024 (1959).
Ryabchuk, V. *Int. J. Photoenergy* **6**, 95 (2004).
Salaices, M., Serrano, B., and de Lasa, H.I. *Chem. Eng. Sci.* **59**, 3 (2004).
Sakai, N., Wang, R., Fujishima, A., Watanabe, T., and Hashimoto, K. *Langmuir* **14**, 5918 (1998).
Satterfield, C.N. "Heterogeneous Catalysis in Practice". McGraw-Hill, New York (1980).
Schiavello, M. (Ed.), "Heterogeneous Photocatalysis". Wiley, New York (1997).
Serpone, N., and Emeline, A.V. *Int. J. Photoenergy* **4**, 91 (2002).
Solonitzyn, Yu.P., Prudnikov, I.M., and Yurkin, V.M. *Russ. J. Phys. Chem.* **57**, 2028 (1982).
Solonitzyn, Yu.P., and Terenin, A.N. *Discuss Faraday. Soc.* **28**, 28 (1959).
Takeuchi, M., Sakamoto, K., Martra, G., Coluccia, S., and Anpo, M.*J. Phys. Chem. B* **109**, 15422 (2005).
Turchi, C.S., and Ollis, D.F. *J. Catal.* **119**, 483 (1989).
Vorontsov, A.V., Kurkin, E.N., and Savinov, E.N. *J. Catal.* **186**, 318 (1999).
Yurdakal, S., Palmisano, G., Loddo, V., Augugliaro, V., and Palmisano, L. *J. Am. Chem. Soc.* **130**, 1568 (2008a).
Yurdakal, S., Loddo, V., Palmisano, G., Augugliaro, V., and Palmisano, L. *Catal. Today*, DOI:10.1016/j.cattod.2008.06.032, (2008b).
Wang, R., Hashimoto, K., Fujishima, A., Chikuni, M., Kojima, E., Kitamura, A., Shimohigoshi, M., and Watanabe, T. *Nature* **388**, 431 (1997).
Wang, R., Sakai, N., Fujishima, A., Watanabe, T., and Hashimoto, K. *J. Phys. Chem. B* **103**, 2188 (1999).
Watanabe, T., Nakajima, A., Wang, R., Minabe, M., Koizumi, S., Fujishima, A., and Hashimoto, K. *Thin Solid Films* **351**, 260 (1999).
Wu, W.C., Liao, L.F., Shiu, J.S., and Lin, J.L. *Phys. Chem. Chem. Phys.* **2**, 4441 (2000).